Supporting Information

Covalently encapsulating sulfur chains into carbon-rich nanomaterials towards high-capacity and high-rate sodium-ion storage

Xinying Luo[a, b], Linlin Ma[a], Ziye Li[a], Xiaoxian Zhao[a], Yanli Dong[a], Qi Yang[c], Huimin Liu[a], Bin Wang[b, *], Linjie Zhi[b, *], and Zhichang Xiao[a, *]

[a]Department of Chemistry, College of Science, Hebei Agricultural University, Baoding 071001, People's Republic of China

[b]CAS Key Laboratory of Nanosystem and Hierarchical Fabrication, CAS Center for Excellence in Nanoscience, National Center for Nanoscience and Technology, Beijing 100190, People's Republic of China

[c]Center for Aircraft Fire and Emergency, Department of Safety Engineering, Civil Aviation University of China, Tianjin 300300, People's Republic of China

*Corresponding author. E-mail: xiaozhichangcnu@sina.cn (Z. Xiao); wangb@nanoctr.cn (B. Wang); zhilj@nanoctr.cn (L. Zhi)

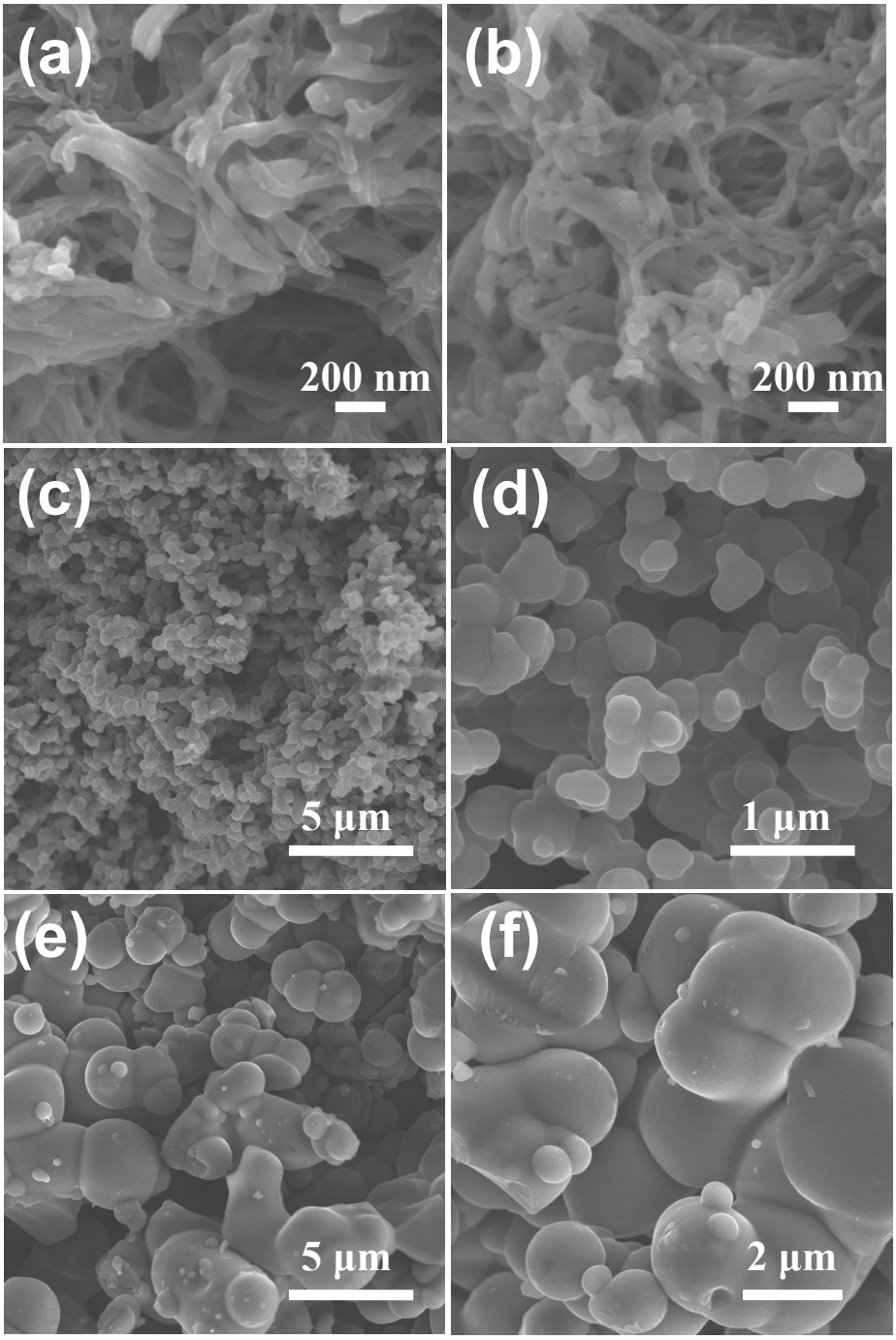

Figure S1. SEM images of (a) KEC-400; (b) KEC-800; (c-d) KFC-600 and (e-f) KTC-600.

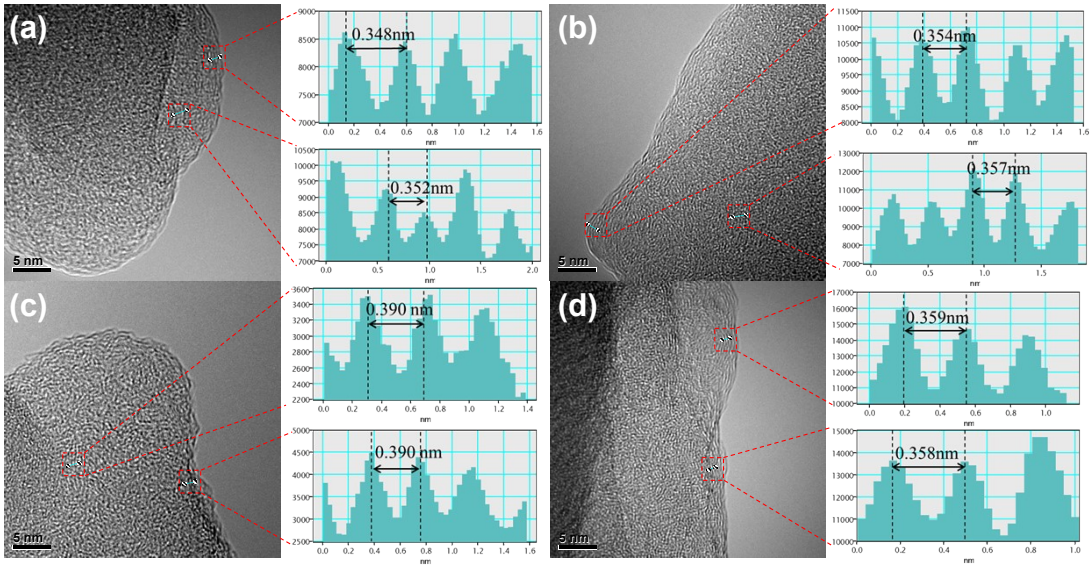

Figure S2. HRTEM images of (a) KEC-400; (b) KEC-800; (c) KTC-600 and (d) KFC-600 with the corresponding intensity profiles for the lines across the selected lattice fringes.

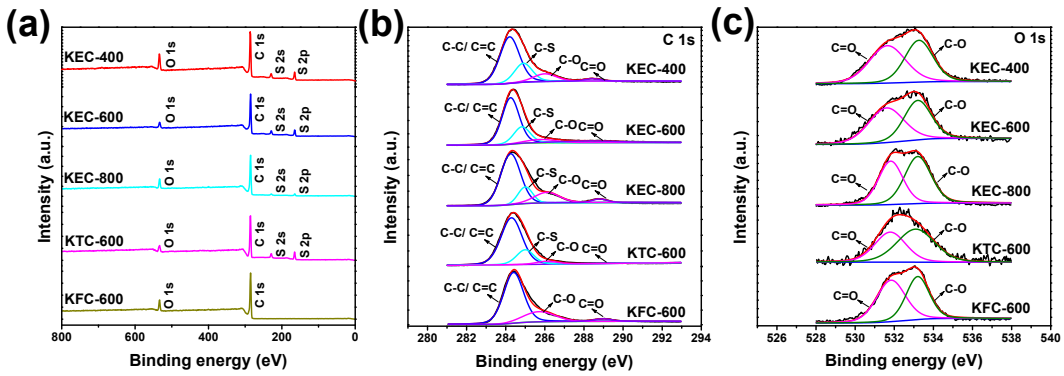

Figure S3. (a) XPS survey spectra, (b) the high-resolution C 1s XPS spectra, (c) the high-resolution O 1s XPS spectra of KEC-400, KEC-600, KEC-800, KTC-600 and KFC-600.

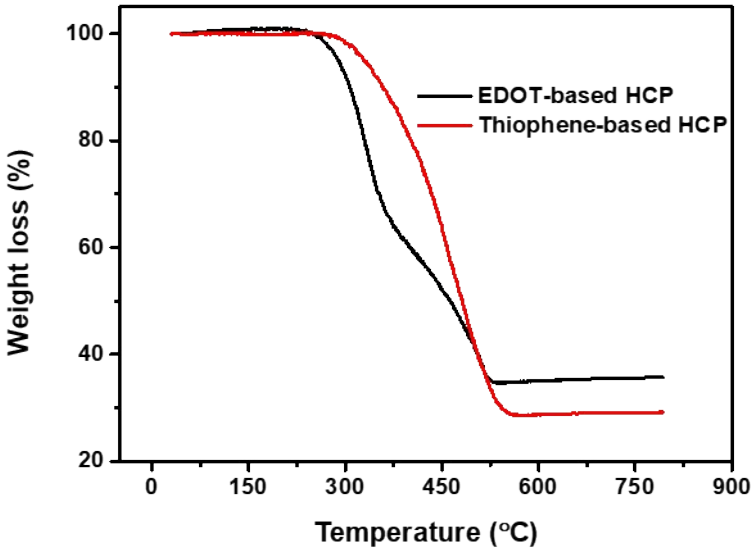

Figure S4. TGA curves of the EDOT-based HCP (black) and thiophene-based HCP (red) from room temperature to 800 ºC under argon atmosphere.

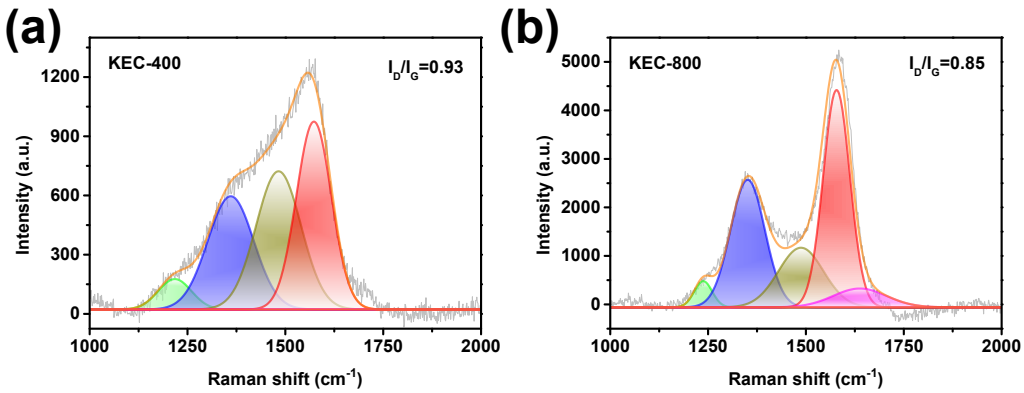

Figure S5. Raman spectra of KEC-400 and KEC-800.

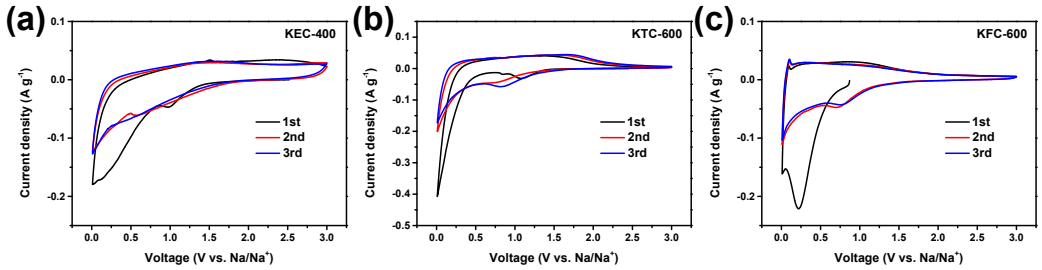

Figure S6. CV curves of (a) KEC-400, (b) KTC-600 and (c) KFC-600 between 0.01-3.0 V at a scan rate of 0.1 mV s^{-1} for the first three cycles.

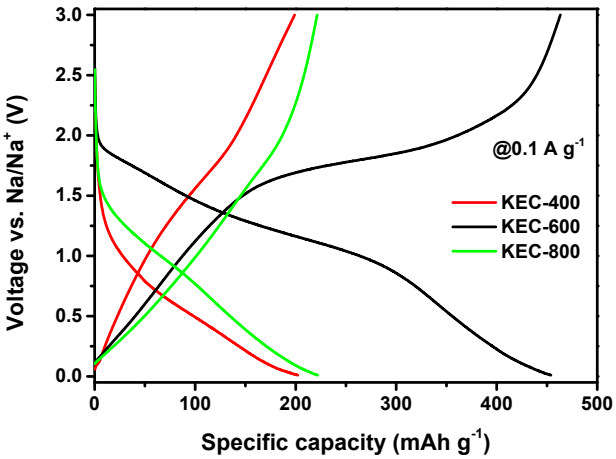

Figure S7. GCD curves of KEC-400, KEC-600 and KEC-800 for their second cycle between 0.01-3.0 V (vs. Na/Na^+) at a current density of 0.1 A g^{-1}.

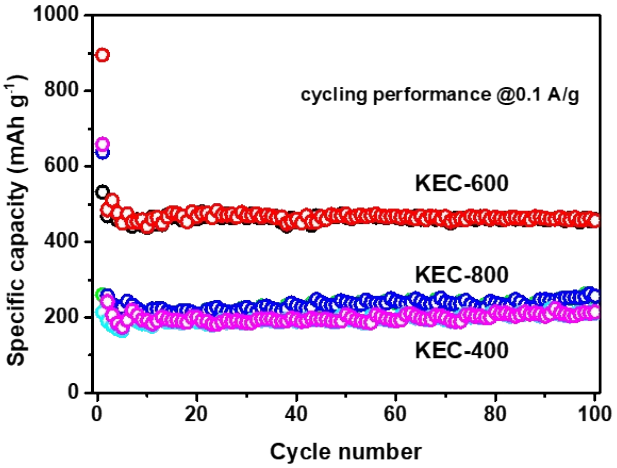

Figure S8. Cycling performance of KEC-400, KEC-600 and KEC-800 at 0.1 A g^{-1}.

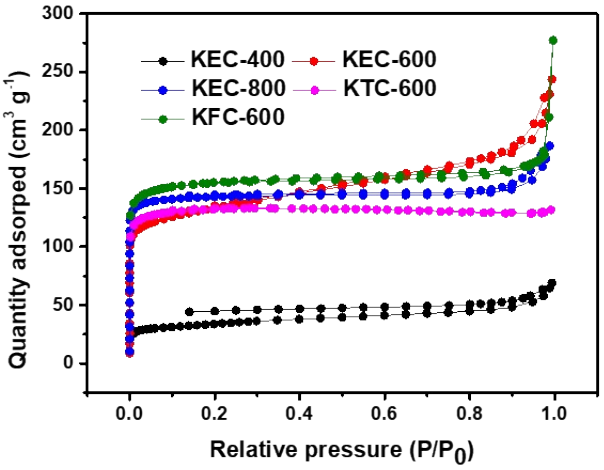

Figure S9. Nitrogen adsorption/desorption isotherms of the samples.

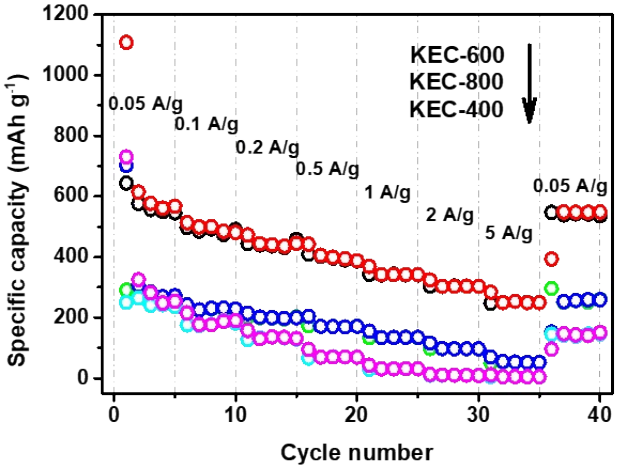

Figure S10. Rate capabilities of KEC-400, KEC-600 and KEC-800 at the current densities of 0.05, 0.1, 0.2, 0.5, 1, 2 and 5 A g^{-1}.

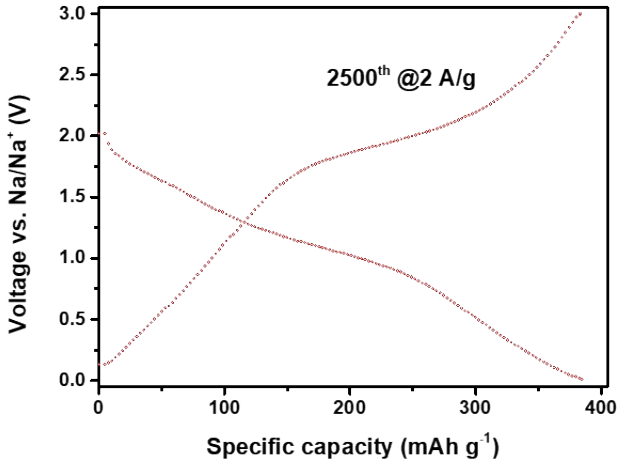

Figure S11. GCD curves of KEC-600 for its 2500th cycle between 0.01-3.0 V (vs. Na/Na^{+}) at a current density of 2 A g^{-1}.

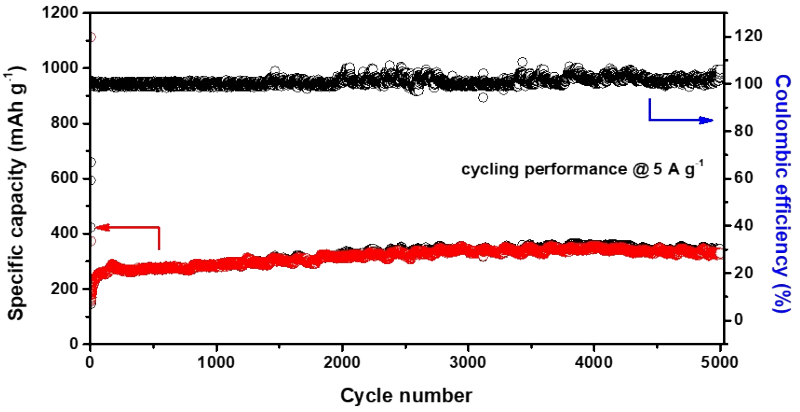

Figure S12. Cycling performance of KEC-600 at 5 A g^{-1} for 5000 cycles.

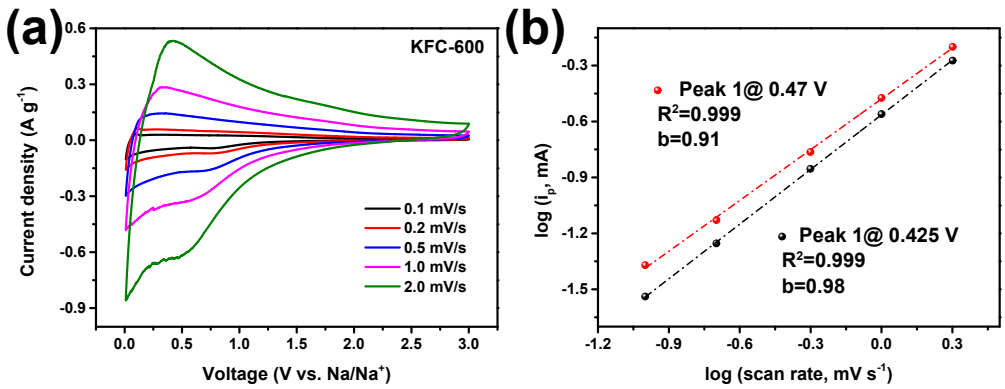

Figure S13. (a) CV curves of KFC-600 at different scan rates ranging from 0.1 to 2 mV s^{-1}; (b) the log(i)-log(v) plots for the determination of b-values based on CV curves.

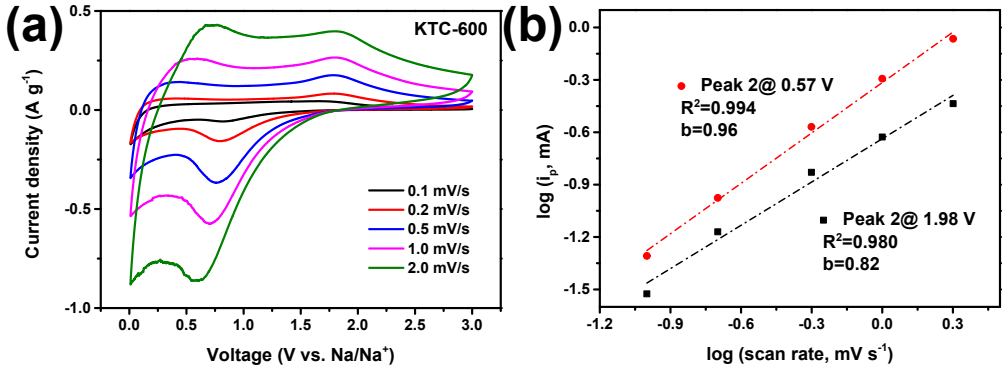

Figure S14. (a) CV curves of KTC-600 at different scan rates ranging from 0.1 to 2 mV s^{-1}; (b) the log(i)-log(v) plots for the determination of b-values based on CV curves.

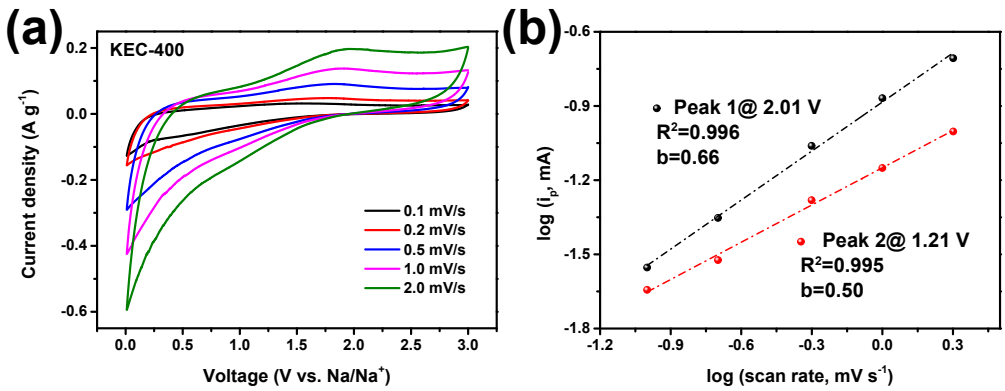

Figure S15. (a) CV curves of KEC-400 at different scan rates ranging from 0.1 to 2 mV s^{-1}; (b) the log(i)-log(v) plots for the determination of b-values based on CV curves.

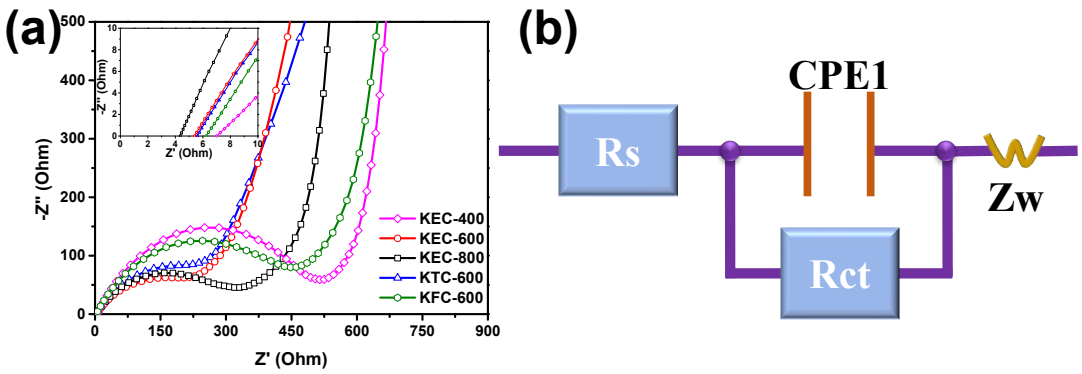

Figure S16. (a) Nyquist plots of KEC-400, KEC-600, KEC-800, KTC-600 and KFC-600 electrodes. The inset illustrates the intercepts of the EIS with Z' axis; (b) equivalent circuits corresponding to the Nyquist plots.

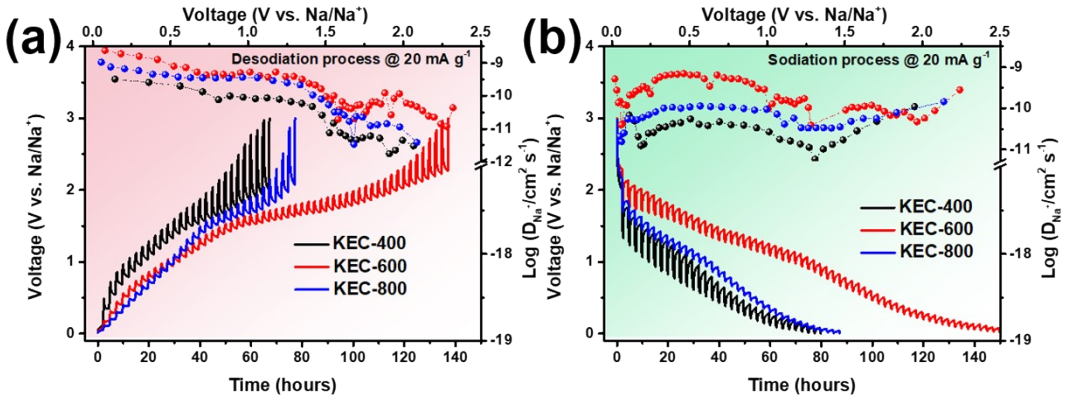

Figure S17. (a) Desodiation process and (b) sodiation process of GITT profiles and the calculated Na^+ diffusion coefficients for KEC-400, KEC-600 and KEC-800 at 20 mA g^{-1}.

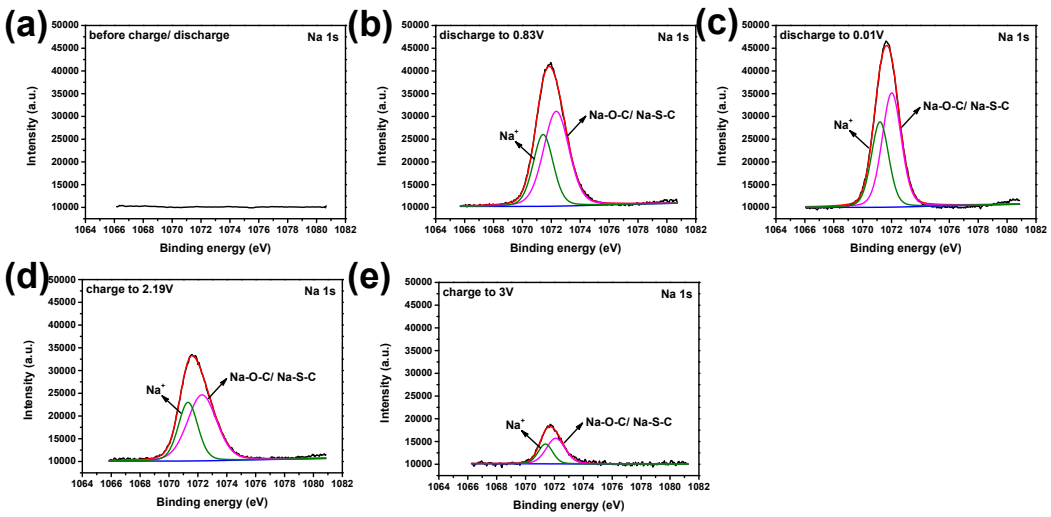

Figure S18. *Ex-situ* Na 1s XPS spectra at the designated voltages.

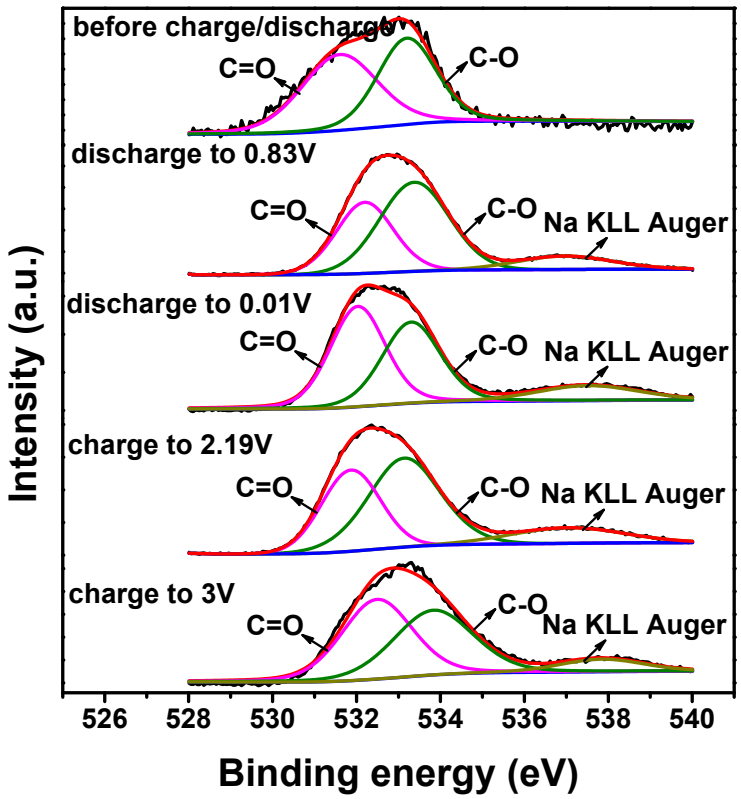

Figure S19. *Ex-situ* O 1s XPS spectra at the designated voltages.

Table S1. XPS results of carbon, sulfur and oxygen elements ratio and the calculated S-S bond ratio according to the integral area of the related peaks.

Samples	C (at%)	S (at%)	O (at%)	ratio of S-S (%)
KEC-400	80.469	7.457	12.074	32.18
KEC-600	86.188	8.216	5.596	58.33
KEC-800	88.449	2.600	8.951	35.80
KTC-600	91.602	6.923	1.475	37.77
KFC-600	91.508	0	8.492	0

Table S2. Elemental analysis (EA) results of sulfur contents and the calculated mass ratio of S-S chains based on the XPS deconvolution results.

Sample	Sulfur content (wt%)	Mass ratio of S-S chain (wt%)
KEC-400	19.25	6.19
KEC-600	21.33	12.44
KEC-800	7.84	2.80
KTC-600	17.10	6.46

Table S3. Detailed data analyzed from the XRD and Raman patterns and the SSA of the samples.

Samples	2 theta (degree)	d-space (nm)	I_D/I_G	SSA (m^2 g^{-1})
KEC-400	25.78	0.345	0.93	125.9
KEC-600	22.29	0.398	1.37	501.0
KEC-800	25.26	0.352	0.85	581.7
KTC-600	22.89	0.388	1.20	407.5
KFC-600	25.04	0.355	0.81	483.0

Table S4. Comparison of the samples for capacity contribution at different voltage regions, rate retention at different current densities and ICE at 0.1 A g^{-1}.

Samples	Capacity contribution @ Low voltage region	Capacity contribution @ High voltage region	Rate retention (%)	Specific capacity @ 5 A g^{-1}	Specific capacity @ 0.05 A g^{-1}	ICE @0.1 A g^{-1} (%)
KEC-400	136.5	65.1	2.0	5	253.9	32.48
KEC-600	148.2	305.2	45.1	253.2	561.3	59.42
KEC-800	129.7	91.7	19.0	52	273.1	40.73
KTC-600	142	130.1	34.8	108	310.4	46.49
KFC-600	116.6	12.3	7.5	12	160.5	33.03

Table S5. Parameters to evaluate the electronic conductivity and charge transfer kinetics for all the samples: Rs and Rct values are obtained from the Nyquist plots; electrical conductivities are obtained by the four-point probe method.

Samples	**Rs (Ω)**	**Rct (Ω)**	**Electrical conductivity (S cm^{-1})**
KEC-400	7.02	523.29	0.94
KEC-600	5.40	225.80	5.78
KEC-800	4.36	330.61	7.61
KTC-600	5.60	241.42	5.07
KFC-600	6.24	460.44	4.03

Table S6. Comparison of the reported SIB performance based on different S-doped carbonaceous anodes.

Samples	**Sulfur contents**	**Current density (A g^{-1})**	**Cycling number**	**Specific capacity (mAh g^{-1})**	**Rate capability**	**References**
Kintting-EDOT derived carbon fibrous clusters	21.33 wt%	2	2500	383.4	253.2 mAh g^{-1} @ 5 A g^{-1}	**This work**
Sulfur-doped disordered carbon	~26.9 wt%	1	1000	271	158 mAh g^{-1} @ 4 A g^{-1}	1
N/S codoped carbon microspheres	---	0.5	3400	150	131 mAh g^{-1} @ 5 A g^{-1}	2
Sulfur-doped graphene foam	5.3 at%	0.05	200	472	168 mAh g^{-1} @ 2 A g^{-1}	3
S-doped N-rich carbon nanosheets	9.19 wt%	1	1000	211	150 mAh g^{-1} @ 5 A g^{-1}	4
Sulfur-doped graphitic carbon nanosheets	2.12 wt%	5	5000	161.8	182.4 mAh g^{-1} @ 3.2 A g^{-1}	5

Sulfur-doped carbon	15.17 wt%	0.5	700	303.2	119.5 mAh g^{-1} @ 5 A g^{-1}	6
S-Doped hard carbon	6.3 at%	1	4000	200	145 mAh g^{-1} @ 5 A g^{-1}	7
S and N codoped interconnected thin carbon shells	---	1.6	4500	200	266.6 mAh g^{-1} @ 4 A g^{-1}	8
N, S-co-doped hierarchical porous carbon	1.63 wt%	1	100	134	95 mAh g^{-1} @ 5 A g^{-1}	9
Sulfur/oxygen dual-functionalized porous carbon-based material	5.15 at%	1	4800	373	165 mAh g^{-1} @ 3.2 A g^{-1}	10
Sulfur and nitrogen codoped mesoporous hollow carbon spheres	2.94 at%	20	7000	180	157 mAh g^{-1} @ 5 A g^{-1}	11
Sulfur covalently bonded graphene	2.52 wt%	1	200	150	83 mAh g^{-1} @ 5 A g^{-1}	12

Sulfur-doped carbon spheres	11.5 at%	1	600	238.2	294.9 mAh g^{-1} @ 2.5 A g^{-1}	13
Sulfur-functionalized graphene monoliths	11.8 wt%	0.5	150	173	123 mAh g^{-1} @ 5 A g^{-1}	14
Sulfur-incorporated carbon material	7.97 at%	1	200	290	255 mAh g^{-1} @ 1 A g^{-1}	15
N/S dual doping porous carbonaceous materials	14.8 at%	2	2000	323	64.5% rate performance @ 2 A g^{-1}	16
Carbon particles doped by N, S elements	---	1	2000	223	132 mAh g^{-1} @ 5 A g^{-1}	17

References:

1 Li W., Zhou M., Li H., Wang K., Cheng S., Jiang K., *Energy Environ. Sci.*, 2015, **8**, 2916-2921.

2 Xu D., Chen C., Xie J., Zhang B., Miao L., Cai J., Huang Y., Zhang L., *Adv. Energy Mater.*, 2016, **6**, 1501929.

3 Islam M. M., Subramaniyam C. M., Akhter T., Faisal S. N., Minett A. I., Liu H. K., Konstantinov K., Dou S. X., *J. Mater. Chem. A*, 2017, **5**, 5290-5302.

4 Yang J., Zhou X., Wu D., Zhao X., Zhou Z., *Adv. Mater.*, 2017, **29**, 1604108.

5 Zou G., Wang C., Hou H., Wang C., Qiu X., Ji X., *Small*, 2017, **13**, 1700762.

6 Qie L., Chen W., Xiong X., Hu C., Zou F., Hu P., Huang Y., *Adv. Sci.*, 2015, **2**, 1500195.

7 Hong Z., Zhen Y., Ruan Y., Kang M., Zhou K., Zhang J.-M., Huang Z., Wei M., *Adv. Mater.*, 2018, **30**, 1802035.

8 Mahmood A., Li S., Ali Z., Tabassum H., Zhu B., Liang Z., Meng W., Aftab W., Guo W., Zhang H., Yousaf M., Gao S., Zou R., Zhao Y., *Adv. Mater.*, 2019, **31**, 1805430.

9 Shao W., Hu F., Song C., Wang J., Liu C., Weng Z., Jian X., *J. Mater. Chem. A*, 2019, **7**, 6363-6373.

10 Wu T., Ling M., Tian Y., Yang L., Hu J., Cao X., Zou G., Hou H., Ji X., *Adv. Funct. Mater.*, 2019, **29**, 1900941.

11 Ni D., Sun W., Wang Z., Bai Y., Lei H., Lai X., Sun K., *Adv. Energy Mater.*, 2019, **9**, 1900036.

12 Wang X., Li G., Hassan F. M., Li J., Fan X., Batmaz R., Xiao X., Chen Z., *Nano Energy*, 2015, **15**, 746-754.

13 Tang H., Yan D., Lu T., Pan L., *Electrochim. Acta*, 2017, **241**, 63-72.

14 Zheng D., Zhang J., Lv W., Cao T., Zhang S., Qiu D., Tao Y., He Y., Kang F., Yang Q.-H., *Chem. Commun.*, 2018, **54**, 4317-4320.

15 Tzadikov J., Levy N. R., Abisdris L., Cohen R., Weitman M., Kaminker I.,

Goldbourt A., Ein-Eli Y., Shalom M., *Adv. Funct. Mater.*, 2020, **30**, 2000592.

16 Lu Y., Liang J., Hu Y., Liu Y., Chen K., Deng S., Wang D., *Adv. Energy Mater.*, 2020, **10**, 1903312.

17 Jin Q., Wang K., Feng P., Zhang Z., Cheng S., Jiang K., *Energy Storage Mater.*, 2020, **27**, 43-50.